J|A|C|S ARTICLES

Published on Web 10/21/2010

Inducing Single-Molecule Magnetism in a Family of Loop-of-Loops Aggregates: Heterometallic $Mn_{40}Na_4$ Clusters and the Homometallic Mn_{44} Analogue

Eleni E. Moushi,[†] Christos Lampropoulos,[‡] Wolfgang Wernsdorfer,[§] Vassilios Nastopoulos,[||] George Christou,*[,‡] and Anastasios J. Tasiopoulos*[,†]

Department of Chemistry, University of Cyprus, 1678 Nicosia, Cyprus, Department of Chemistry, University of Florida, Gainesville, Florida 32611-7200, United States, Institut Néel, CNRS, BP 166, 38042 Grenoble Cedex 9, France, and Department of Chemistry, University of Patras, 26504 Patras, Greece

Received July 27, 2010; E-mail: christou@chem.ufl.edu; atasio@ucy.ac.cy

Abstract: The syntheses, crystal structures, and magnetic properties of a new family of heterometallic $Mn_{40}Na_4$ and homometallic Mn_{44} loop-of-loops aggregates are reported. The reactions of $[Mn_3O(O_2CMe)_6(py)_3]\cdot py$ with 1,3-propanediol (pdH_2) and 2-methyl-1,3-propanediol ($mpdH_2$) in the presence of NaN_3 afforded $[Mn_{10}Na(\mu_3\text{-}O)_2(O_2CMe)_{13}(pd)_6(py)_2]_4$ (**1**)$_4$ and $[Mn_{10}Na(\mu_3\text{-}O)_2(O_2CMe)_{13}(mpd)_6(py)(H_2O)]_4$ (**2**)$_4$, respectively. $Mn_{40}Na_4$ complexes (**1**)$_4$ and (**2**)$_4$ consist of four Mn_{10} loops linked through Na^+ ions to give a supramolecular aggregate with a saddle-like topology. Magnetic characterization of compound (**1**)$_4$ showed that each Mn_{10} loop has an $S = 4$ ground-state spin and displays frequency-dependent in-phase and out-of-phase ac susceptibility signals. It also exhibits hysteresis loops that, however, are not typical of single-molecule magnets (SMMs) due to the existence of interloop interactions between the neighboring Mn_{10} units of (**1**)$_4$ through the diamagnetic Na^+ ions, and also intermolecular interactions between different $Mn_{40}Na_4$ aggregates. The magnetically discrete Mn_{44} analogue was targeted with high priority and finally prepared from the reaction of $[Mn_3O(O_2CMe)_6(py)_3]\cdot py$ with pdH_2 in the presence of $Mn(ClO_4)_2\cdot 6H_2O$. The loop-of-loops structure of $[Mn_{44}(\mu_3\text{-}O)_8(O_2CMe)_{52}(pd)_{24}(py)_8](ClO_4)(OH)_3$ (**3**) is essentially identical to those of (**1**)$_4$ and (**2**)$_4$, with the most significant difference being that the four Na^+ ions of (**1**)$_4$ and (**2**)$_4$ have been replaced with Mn^{2+} ions. Compound **3** is thus best described magnetically as a Mn_{44} cluster. In accord with this description and the stronger exchange coupling between the four Mn_{10} loops expected through the connecting Mn^{2+} ions, magnetic susceptibility measurements revealed that **3** has an $S = 6$ ground-state spin and displays frequency-dependent in-phase and out-of-phase ac signals. Magnetization vs dc field sweeps on single-crystals of **3** displayed scan rate- and temperature-dependent hysteresis loops confirming that complex **3** is a new SMM, and is thus the second largest Mn cluster and SMM reported to date.

Introduction

One of the motivating themes in metal cluster chemistry is the synthesis of high-nuclearity complexes of paramagnetic metal ions that can function as nanoscale magnetic materials. Such species have been called single-molecule magnets (SMMs), or molecular nanomagnets, and represent a molecular or "bottom-up" approach to nanoscale magnetism.[1−3] SMMs below their blocking temperature exhibit magnetization hysteresis, the classical macroscale property of a magnet, as well as quantum tunneling of the magnetization (QTM)[3,4] and quantum phase interference,[5] the properties of the microscale. SMMs derive their properties from a combination of a large ground-state spin (S) value and an Ising (easy-axis) type of magnetoanisotropy (negative zero-field splitting parameter, D), which results in a barrier to magnetization relaxation. The upper limit of this is given by $S^2|D|$ and $(S^2 - {}^1/_4)|D|$ for integer and half-integer spin systems, respectively. Many groups around the world have sought to synthesize polynuclear clusters and SMMs of very large dimensions (by molecular standards), comparable to those of the smaller magnetic nanoparticles,[6] with the aim of bridging the molecular (or bottom-up) and classical (or top-down) approaches to nanoscale magnetic materials. As a result of these investigations, several giant homometallic clusters of 3d and

[†] University of Cyprus.
[‡] University of Florida.
[§] Institut Néel, CNRS.
[||] University of Patras.

(1) (a) Sessoli, R.; Tsai, H.-L.; Schake, A. R.; Wang, S.; Vincent, J. B.; Folting, K.; Gatteschi, D.; Christou, G.; Hendrickson, D. N. *J. Am. Chem. Soc.* **1993**, *115*, 1804. (b) Christou, G.; Gatteschi, D.; Hendrickson, D. N.; Sessoli, R. *MRS Bull.* **2000**, *25*, 66. (c) Sessoli, R.; Gatteschi, D.; Ganeschi, A.; Novak, M. A. *Nature* **1993**, *365*, 141. (d) Bagai, R.; Christou, G. *Chem. Soc. Rev.* **2009**, *38*, 1011.
(2) Aromi, G.; Brechin, E. K. *Struct. Bonding (Berlin)* **2006**, 1.
(3) Gatteschi, D.; Sessoli, R. *Angew. Chem., Int. Ed.* **2003**, *42*, 268.
(4) (a) Friedman, J. R.; Sarachik, M. P.; Tejada, J.; Ziolo, R. *Phys. Rev. Lett.* **1996**, *76*, 3830. (b) Thomas, L.; Lionti, F.; Ballou, R.; Gatteschi, D.; Sessoli, R.; Barbara, B. *Nature* **1996**, *383*, 145.
(5) Wernsdorfer, W.; Sessoli, R. *Science* **1999**, *284*, 133.
(6) Jamet, M.; Wernsdorfer, W.; Thirion, C.; Mailly, D.; Dupuis, V.; Mélinon, P.; Pérez, A. *Phys. Rev. Lett.* **2001**, *86*, 4676.

 10.1021/ja106666h

4f paramagnetic metal ions have been isolated, consisting of the metals Mn (Mn_{84}, Mn_{32}, Mn_{30}),[7−9] Fe (Fe_{64}, Fe_{168}),[10] Co (Co_{36}),[11] Ni (Ni_{24}),[12] Cu (Cu_{44}),[13] and Er (Er_{60}).[14] In addition, a number of heterometallic 3d/3d and 3d/4f clusters have been reported, such as $Mn_{28}Cu_{17}$[15] and $Cu_{24}Dy_8$,[16] and also some Ni^{2+}/4f clusters,[17−19] the most impressive of which is a $Ni_{54}Gd_{54}$ cluster.[17] Among these clusters, only Mn_{84}, Mn_{30}, and $Cu_{24}Dy_8$ have been unambiguously proven to display SMM behavior.[7,9a,15,16] Despite the large amount of work that has been performed in this area so far, there are still many challenges to be addressed by chemists. One of them involves the discovery of new giant SMMs comparable to or even larger in size than the Mn_{30}, $Cu_{24}Dy_8$, and Mn_{84} complexes known to date in order to better study and understand the magnetic properties of SMMs which reach the size regime of the traditional (top-down) nanoscale magnetic particles. A second challenge is related to the development of new synthetic strategies for optimization of the magnetic properties of large polynuclear metal compounds. Such methods currently involve preparation of new analogues by applying targeted structural modification of known compounds and have been employed to date mainly with smaller clusters and especially with the Mn_{12}[1,20] and more recently the Mn_6[21] and Mn_3[22] families of SMMs. However, in the chemistry of large polynuclear clusters, there exist only a handful of cases where targeted modification of the structure of a given compound has resulted in derivative(s) with improved magnetic properties.[23] Some examples of such targeted modifications of large clusters include (i) the increase of the spin of a Mn_{25} cluster by modifying its peripheral ligation;[23a] (ii) the increase of the anisotropy of a Mn_{19} cluster with a giant $S = {}^{83}/_{2}$ ground-state spin by preparation of a $Mn_{18}Dy$ complex that contained a Dy^{3+} ion instead of a Mn^{2+} ion;[23b] and (iii) the targeted synthesis of a discrete Mn_{17} SMM with a giant $S = 37$ ground-state spin after the identification of this Mn_{17} unit as a high-spin repeating unit in two polymeric compounds.[23c]

In the present work, we shall describe a family of large molecular aggregates constructed from smaller clusters linked through Na^+ or Mn^{2+} ions. The large tetrameric $[Mn_{10}Na(\mu_3\text{-}O)_2(O_2CMe)_{13}(pd)_6(py)_2]_4$, $(\mathbf{1})_4$ (pdH_2 = 1,3-propanediol), $[Mn_{10}Na(\mu_3\text{-}O)_2(O_2CMe)_{13}(mpd)_6(py)(H_2O)]_4$, $(\mathbf{2})_4$ ($mpdH_2$ = 2-methyl-1,3-propanediol), and $\{[Mn_{11}(\mu_3\text{-}O)_2(O_2CMe)_{13}(pd)_6(py)_2](ClO_4)_{0.25}(OH)_{0.75}\}_4$, **3**, molecular clusters consist of Mn_{10} loops linked through Na^+ [$(\mathbf{1})_4$, $(\mathbf{2})_4$] or Mn^{2+} (**3**) ions and have a saddle-like topology. The two heterometallic $Mn_{40}Na_4$ complexes were the first ones isolated. Magnetic susceptility and hysteresis studies revealed that $(\mathbf{1})_4$ is not a SMM, and its overall magnetic behavior is dramatically influenced by the existence of only weak interloop interactions between the four Mn_{10} loops of a $(\mathbf{1})_4$ aggregate (mediated through the diamagnetic Na^+ ions), comparable with the expected weak intermolecular interactions between different $(\mathbf{1})_4$ aggregates. The isolation of the magnetically discrete, homometallic analogue (Mn_{44}) was thus targeted with high priority as a means of strengthening the interloop interactions and potentially thus yielding structurally and magnetically discrete Mn_{44} clusters that might be new SMMs. This objective was realized by the successful preparation of the Mn_{44} complex **3**. A variety of magnetism studies have established **3** as a new SMM, the second largest SMM and Mn cluster reported to date. The synthesis and study of $(\mathbf{1})_4$ has been previously communicated.[24]

Experimental Details

Syntheses. All manipulations were performed under aerobic conditions using materials as received unless otherwise indicated; water was distilled in-house. $[Mn_3O(O_2CMe)_6(py)_3]\cdot py$ was prepared as previously described.[25] Elemental analyses were performed by the in-house facilities of the Chemistry Department, University of Cyprus. **Warning!** *Although we encountered no problems, appropriate care should be taken in the use of the potentially explosive perchlorate and azide anions.*

$[Mn_{10}Na(\mu_3\text{-}O)_2(O_2CMe)_{13}(pd)_6(py)_2]_4$, $(\mathbf{1})_4$. Method A. To a solution of $[Mn_3O(O_2CMe)_6(py)_3]\cdot py$ (0.294 g, 0.346 mmol) in 20 mL of MeCN were added pdH_2 (0.10 mL, 1.384 mmol) and NaN_3 (0.0225 g, 0.346 mmol), and the solution was then left under magnetic stirring for ∼10 min. The resulting slurry was filtered, and the dark red-brown filtrate was left undisturbed at room temperature. After 2 days, dark red-brown crystals of $(\mathbf{1}\cdot 2.4H_2O)_4$ appeared, suitable for X-ray structural determination. The crystals were isolated by filtration, washed with a copious amount of MeCN,

(7) Tasiopoulos, A. J.; Vinslava, A.; Wernsdorfer, W.; Abboud, K. A.; Christou, G. *Angew. Chem., Int. Ed.* **2004**, *43*, 2117.
(8) Scott, R. T. W.; Parsons, S.; Murugesu, M.; Wernsdorfer, W.; Christou, G.; Brechin, E. K. *Angew. Chem., Int. Ed.* **2005**, *44*, 6540.
(9) (a) Soler, M.; Wernsdorfer, W.; Folting, K.; Pink, M.; Christou, G. *J. Am. Chem. Soc.* **2004**, *126*, 2156. (b) Soler, M.; Rumberger, E.; Folting, K.; Hendrickson, D. N.; Christou, G. *Polyhedron* **2001**, *20*, 1365.
(10) (a) Liu, T.; Zhang, Y.-J.; Wang, Z.-M.; Gao, S. *J. Am. Chem. Soc.* **2008**, *130*, 10500. (b) Zhang, Z.-M.; Yao, S.; Li, Y.-G.; Clérac, R.; Lu, Y.; Su, Z.-M.; Wang, E.-B. *J. Am. Chem. Soc.* **2009**, *131*, 14600.
(11) Alborés, P.; Rentschler, E. *Angew. Chem., Int. Ed.* **2009**, *48*, 9366.
(12) Foguet-Albiol, D.; Abboud, K. A.; Christou, G. *Chem. Commun.* **2005**, 4282.
(13) Murugesu, M.; Clérac, R.; Anson, C. E.; Powell, A. K. *Inorg. Chem.* **2004**, *43*, 7269.
(14) Kong, X.-J.; Wu, Y.; Long, L.-S.; Zheng, L.-S.; Zheng, Z. *J. Am. Chem. Soc.* **2009**, *131*, 6918.
(15) Ac magnetic susceptibility studies on a microcrystalline powder of the $Cu_{17}Mn_{28}$ complex revealed the existence of frequency-dependent signals; however, more studies need to be performed in order to confirm its SMM behavior. Wang, W.-G.; Zhou, A.-J.; Zhang, W.-X.; Tong, M.-L.; Chen, X.-M.; Nakano, M.; Beedle, C. C.; Hendrickson, D. N. *J. Am. Chem. Soc.* **2007**, *129*, 1014.
(16) Baskar, V.; Gopal, K.; Helliwell, M.; Tuna, F.; Wernsdorfer, W.; Winpenny, R. E. P. *Dalton Trans.* **2010**, *39*, 4747.
(17) Kong, X.-J.; Ren, Y.-P.; Chen, W.-X.; Long, L.-S.; Zheng, Z.; Huang, R.-B.; Zheng, L.-S. *Angew. Chem., Int. Ed.* **2008**, *47*, 2398.
(18) Kong, X.-J.; Ren, Y.-P.; Long, L.-S.; Zheng, Z.; Nichol, G.; Huang, R.-B.; Zheng, L.-S. *Inorg. Chem.* **2008**, *47*, 2728.
(19) The largest Ni/4f cluster has been prepared with a diamagnetic 4f ion (La^{3+}): Kong, X.-J.; Long, L.-S.; Huang, R.-B.; Zheng, L.-S.; Harris, T. D.; Zheng, Z. *Chem. Commun.* **2009**, 4354.
(20) Tasiopoulos, A. J.; Wernsdorfer, W.; Abboud, K. A.; Christou, G. *Angew. Chem., Int. Ed.* **2004**, *43*, 6338.
(21) (a) Milios, C. J.; Vinslava, A.; Wernsdorfer, W.; Moggach, S.; Parsons, S.; Perlepes, S. P.; Christou, G.; Brechin, E. K. *J. Am. Chem. Soc.* **2007**, *129*, 2754. (b) Milios, C. J.; Inglis, R.; Vinslava, A.; Bagai, R.; Wernsdorfer, W.; Parsons, S.; Perlepes, S. P.; Christou, G.; Brechin, E. K. *J. Am. Chem. Soc.* **2007**, *129*, 12505. (c) Milios, C. J.; Piligkos, S.; Brechin, E. K. *Dalton Trans.* **2008**, 1809. (d) Feng, P. L.; Hendrickson, D. N. *Inorg. Chem.* **2010**, *49*, 6393.
(22) (a) Stamatatos, T. C.; Foguet-Albiol, D.; Lee, S. C.; Stoumpos, C. C.; Raptopoulou, C. P.; Terzis, A.; Wernsdorfer, W.; Hill, S. O.; Perlepes, S. P.; Christou, G. *J. Am. Chem. Soc.* **2007**, *129*, 9484. (b) Inglis, R.; Taylor, S. M.; Jones, L. F.; Papaefstathiou, G. S.; Perlepes, S. P.; Datta, S.; Hill, S.; Wernsdorfer, W.; Brechin, E. K. *Dalton Trans.* **2009**, 9157.
(23) (a) Stamatatos, T. C.; Abboud, K. A.; Wernsdorfer, W.; Christou, G. *Angew. Chem., Int. Ed.* **2007**, *46*, 884. (b) Ako, A. M.; Mereacre, V.; Clérac, R.; Wernsdorfer, W.; Hewitt, I. J.; Anson, C. E.; Powell, A. K. *Chem. Commun.* **2009**, 544. (c) Moushi, E. E.; Stamatatos, T. C.; Wernsdorfer, W.; Nastopoulos, V.; Christou, G.; Tasiopoulos, A. J. *Inorg. Chem.* **2009**, *48*, 5049.
(24) Moushi, E. E.; Lampropoulos, C.; Wernsdorfer, W.; Nastopoulos, V.; Christou, G.; Tasiopoulos, A. J. *Inorg. Chem.* **2007**, *46*, 3795.
(25) Vincent, J. B.; Chang, H.-R.; Folting, K.; Huffman, J. C.; Christou, G.; Hendrickson, D. N. *J. Am. Chem. Soc.* **1987**, *109*, 5703.

Table 1. Crystallographic Data for Complexes (**1**·2.4H_2O)$_4$, (**1**·2.5CH_2Cl_2)$_4$ (**2**·H_2mpd·2.5H_2O)$_4$, and **3**·(6 + *x*)H_2O

parameter	(**1**·2.4H_2O)$_4$	(**1**·2.5CH_2Cl_2)$_4$	(**2**·H_2mpd·2.5H_2O)$_4$	**3**·(6 + *x*)H_2O
formula[a]	$C_{216}H_{359.2}O_{169.60}N_8Na_4Mn_{40}$	$C_{226}H_{360}Cl_{20}O_{160}N_8Na_4Mn_{40}$	$C_{236}H_{436}O_{182}N_4Na_4Mn_{40}$	$C_{216}H_{355}O_{173}N_8ClMn_{44}$
fw, g mol^{-1}	8071.49	8747.80	8531.45	8284.89
crystal system	tetragonal	tetragonal	tetragonal	tetragonal
space group	$I4_1/a$	$P\bar{4}2_1c$	$I4_1/acd$	$I4_1/a$
a, Å	25.0996(5)	25.8279(4)	34.5332(4)	23.9377(3)
b, Å	25.0996(5)	25.8279(4)	34.5332(4)	23.9377(3)
c, Å	70.929(2)	33.825(2)	100.381(2)	70.072(2)
V, Å^3	44685(2)	22564.3(9)	119709(3)	40152(2)
Z	4	2	8	4
T, K	100(2)	100(2)	100(2)	100(2)
radiation, Å[b]	0.71073	0.71073	0.71073	0.71073
ρ_{calc}, g cm^{-3}	1.197	1.288	0.947	1.371
μ, mm^{-1}	1.160	1.268	0.870	1.415
R1, %[c]	5.45	6.79	9.54	6.64
wR2, %[d]	15.37	15.17	25.47	15.97

[a] Including solvent molecules. [b] Graphite monochromator. [c] $R1 = \sum(||F_o| - |F_c||)/\sum|F_o|$. [d] $wR2 = [\sum[w(F_o^2 - F_c^2)^2]/\sum[wF_o^2)^2]]^{1/2}$, where $w = 1/[\sigma^2(F_o^2) + (mp)^2 + np]$, $p = [\max(F_o^2,0) + 2F_c^2]/3$, and *m* and *n* are constants.

and dried in vacuo; the yield was ∼32%. The crystals used for single-crystal X-ray crystallography were maintained in contact with the mother liquor to prevent loss of interstitial solvent. Dried solid was hygroscopic and analyzed as (**1**·10H_2O)$_4$. Anal. Calcd (found) for (**1**·10H_2O)$_4$ ($C_{216}H_{420}O_{200}N_8Na_4Mn_{40}$): C, 30.10 (29.90); H, 4.91 (4.76); N, 1.30 (1.20). Selected IR data (cm^{-1}, KBr pellet): 3417(s, br), 2945(w), 2866(w), 1589(s, br), 1418(s, br), 1339(w), 1054(s), 941(w), 835(s), 665(s), 615(s), 584(w).

Method B. Method A was repeated using CH_2Cl_2 as reaction solvent instead of MeCN. The resulting slurry was filtered, and the dark red-brown filtrate was divided into small portions (3 mL each), each of which was layered with Et_2O (1:3 ratio). After 2 weeks, dark red-brown crystals of (**1**·2.5CH_2Cl_2)$_4$ appeared and were left to grow for a few more days to give X-ray-quality crystals. These were isolated by filtration, washed with CH_2Cl_2 (40 mL), and dried in vacuo; the yield was ∼29%. The crystals for X-ray studies were maintained in contact with mother liquor.

Method C. Method A was repeated using NaCN, NaOCN, NaSCN, or Na[$N(CN)_2$] in place of NaN_3. The yields were in the 18−26% range. The products were identified as (**1**·2.4H_2O)$_4$ by IR spectral comparison with authentic material and from unit cell determinations.

Method D. Method A was repeated but with small portions (2 mL) of MeOH or pyridine added to the reaction solution. In each case, the product was identified as (**1**·2.4H_2O)$_4$ by IR spectral comparison with authentic material and from unit cell determinations. The yields were ∼24 and 26%, respectively.

[$Mn_{10}Na(\mu_3$-O)$_2$(O_2CMe)$_{13}$(mpd)$_6$(py)(H$_2$O)], (2)$_4$. To a slurry of [$Mn_3O(O_2CMe)_6(py)_3$]·py (0.319 g, 0.375 mmol) in 15 mL of CH_2Cl_2 were added H_2mpd (0.10 mL, 1.126 mmol) and NaN_3 (0.0244 g, 0.375 mmol), and the mixture was left under magnetic stirring for ∼5 min. The resulting slurry was filtered, and the dark red-brown filtrate was divided into small portions (∼3 mL each), each of which was layered with *n*-hexane (1:3 ratio). After a few weeks, dark red-brown crystals of (**2**·H_2mpd·2.5H_2O)$_4$ appeared and were left to grow for a few more weeks to give X-ray-quality crystals. The crystals were isolated by filtration, washed with CH_2Cl_2 (40 mL), and dried in vacuo; the yield was ∼23%. The crystals for X-ray studies were again maintained in contact with mother liquor. Dried solid was hygroscopic and analyzed as (**2**·H_2mpd·13H_2O)$_4$. Anal. Calcd (found) for (**2**·H_2mpd·13H_2O)$_4$ ($C_{236}H_{520}O_{224}N_4Na_4Mn_{40}$): C, 30.52 (30.38); H, 5.64 (5.48); N, 0.60 (0.52). Selected IR data (cm^{-1}, KBr pellet): 3414(s, br), 2961(w), 2925(w), 2852(w), 1562(s, br), 1421(s, br), 1343(w), 1058(s), 943(w), 835(s), 669(s), 617(s), 593(w).

[$Mn_{44}(\mu_3$-O)$_8$(O_2CMe)$_{52}$(pd)$_{24}$(py)$_8$](ClO$_4$)(OH)$_3$, 3. To a slurry of [$Mn_3O(O_2CMe)_6(py)_3$]·py (0.236 g, 0.277 mmol) in 20 mL of CH_2Cl_2 were added pdH_2 (0.10 mL, 1.384 mmol) and $Mn(ClO_4)_2$·6H_2O (0.100 g, 0.277 mmol), and the mixture was left under magnetic stirring for ∼8 h. The resulting slurry was filtered, and the dark red-brown filtrate was divided into small portions (3 mL each), each of which was layered with Et_2O (1:3 ratio). Within 1 day, well-formed hexagonal and plate crystals appeared and were left to grow for a few more days to give X-ray-quality crystals. The hexagonal crystals were identified crystallographically as **3**·(6 + *x*)H_2O, whereas the plate crystals proved to be poor diffractors of X-rays. The large hexagonal crystals were separated manually from the plate crystals (in paratone-N oil), washed with a copious amount of heptane and then with Et_2O (20 mL), and dried in vacuo; the yield was ∼25%. The crystals for X-ray crystallography were again maintained in contact with mother liquor. Dried solid was hygroscopic and analyzed as **3**·60H_2O. Anal. Calcd (found) for **3**·60H_2O ($C_{216}H_{463}O_{227}N_8ClMn_{44}$): C, 28.02 (27.89); H, 5.04 (4.93); N, 1.21 (1.10). Selected IR data (cm^{-1}, KBr pellet): 3449(s, br), 2930(w), 2866(w), 1587(s, br), 1412(s, br), 1342(w), 1094 (m), 1061(s), 947(w), 833(s), 669(s), 621(s), 580(w).

X-ray Crystallography. Data were collected on an Oxford Diffraction diffractometer, equipped with a CCD area detector and a graphite monochromator utilizing Mo Kα radiation ($\lambda = 0.71073$ Å). Suitable crystals were attached to glass fibers using paratone-N oil and transferred to a goniostat where they were cooled for data collection. Unit cell dimensions were determined and refined by using 53 734 ($3.04 \le \theta \le 28.55°$), 17 545 ($2.98 \le \theta \le 30.57$), 45 048 ($3.03 \le \theta \le 29.37°$), and 38 243 ($3.00 \le \theta \le 30.46°$) reflections for (**1**·2.4H_2O)$_4$, (**1**·2.5CH_2Cl_2)$_4$, (**2**·H_2mpd·2.5H_2O)$_4$, and **3**·(6 + *x*)H_2O, respectively. Empirical absorption corrections (multiscan based on symmetry-related measurements) were applied using CrysAlis RED software.[26] The structures were solved by direct methods using SIR92[27a] and refined on F^2 using full-matrix least-squares using SHELXL97.[27b] Programs used: CrysAlis CCD[26] for data collection, CrysAlis RED[26] for cell refinement and data reduction, and DIAMOND[28a] and MERCURY[28b] for molecular graphics. The non-H atoms were treated anisotropically, whereas the hydrogen atoms were placed in calculated, ideal positions and refined as riding on their respective carbon atoms. Unit cell data and structure refinement details are listed in Table 1. Full details can be found in the CIF files provided in the Supporting Information.

For all four complexes, the asymmetric unit consists of a (Mn_{10}M) (M = Na^+, **1** and **2**; M = Mn^{2+}, the Mn_{11} loop of **3**) loop plus solvent molecules and, for **3**·(6 + *x*)H_2O, counterions (0.25ClO_4^- and 0.75OH^-). **3**·(6 + *x*)H_2O also contains severely disordered lattice H_2O molecules that could not be modeled properly; thus the program SQUEEZE, a part of the PLATON

(26) Oxford Diffraction. *CrysAlis CCD and CrysAlis RED*, version p171.33.34d; Oxford Diffraction Ltd.: Abingdon, Oxford, England, 2009.

package of crystallographic software, was used to calculate the solvent disorder area and remove its contribution from the intensity data.[29]

Direct Current and Alternating Current Magnetometry. Variable-temperature dc magnetic susceptibility data down to 1.80 K were collected on a Quantum Design MPMS-XL SQUID magnetometer equipped with a 70 kG (7 T) dc magnet at the University of Florida. Diamagnetic corrections were applied to the observed paramagnetic susceptibilities using Pascal's constants. Samples were embedded in solid eicosane to prevent torquing in the dc field. Ac magnetic susceptibility data were collected on the same instrument employing a 3.5 G ac field oscillating at frequencies up to 1500 Hz. Magnetization vs field and temperature data were fit using the program MAGNET.[30] Studies at ultralow temperatures (<1.8 K) were performed on single crystals at Grenoble using an array of micro-SQUIDs.[31] The high sensitivity of this magnetometer allows the study of single crystals of the order of 10−500 μm; the field can be applied in any direction by separately driving three orthogonal coils.

Other Studies. IR spectra were recorded on KBr pellets in the 4000−400 cm^{-1} range using a Shimadzu Prestige-21 spectrometer.

Results and Discussion

Syntheses. We have been systematically investigating over the past few years the use of pdH_2 and $mpdH_2$ in Mn carboxylate chemistry as a route to new polynuclear metal clusters and SMMs. One reaction system has involved the use of both (m)pdH_2 and N_3^- ligands, and it has led to a discrete Mn_{17} octahedral cluster with a giant $S = 37$ ground-state spin, two multidimensional coordination polymers of this Mn_{17} unit,[23c] and Mn_8 rod-like clusters.[32] This reaction system is capable of giving products containing both N_3^- and (m)pd^{n-} ($n = 0$, 1, or 2) ligands, but also ones containing only one of these. In the present work, the products $(\mathbf{1})_4$, $(\mathbf{2})_4$, and **3** are members of the latter category since they were prepared in the presence of N_3^- but contain only pd^{2-} or mpd^{2-} groups. Thus, reaction of $[Mn_3O(O_2CMe)_6(py)_3]\cdot py$ with pdH_2 and NaN_3 in a 1:4:1 molar ratio in MeCN resulted in the isolation of $(\mathbf{1})_4$, crystallizing as $(\mathbf{1}\cdot 2.4H_2O)_4$ in 32% yield. Since $(\mathbf{1})_4$ contains Na^+ but not N_3^-, we assumed that NaN_3 was important merely as the source of Na^+ and perhaps to provide additional weak base (N_3^-) for oxide ion formation. This was supported by the same reactions but with NaCN, NaOCN, NaSCN, or $Na[N(CN)_2]$ instead of NaN_3, which all gave $(\mathbf{1})_4$ as the isolated product (identified by IR spectral comparison with authentic material and from unit cell determinations), but in slightly lower yields (18−26%). However, when $NaClO_4$ or $NaNO_3$ was used in place of NaN_3, crystals of the 3-D coordination polymer $\{[Mn_{19}Na(\mu_4\text{-}O)_9(\mu_3\text{-}O)(\mu_3\text{-}OH)_3(O_2CMe)_9(L)_9(H_2O)_3](OH)\}_\infty$ (L = pd, **4**; L = mpd, **5**) were isolated.[33] Similar reactions with other Na^+-containing salts, such as NaCl, NaBr, and Na_2SO_4, gave microcrystalline solids that we were unable to characterize further.

Some other modifications to the reaction were also investigated: (i) addition of a small amount of MeOH (to potentially provide MeO^--containing product) or extra pyridine and (ii) use of CH_2Cl_2 rather than MeCN as the reaction solvent. In all cases, however, the product was $(\mathbf{1})_4$ in yields ∼24−29%, but in case (ii) the compound crystallized as $(\mathbf{1}\cdot 2.5CH_2Cl_2)_4$. Similar modifications were also performed with $mpdH_2$ in place of pdH_2. In this case, $(\mathbf{2})_4$ was isolated only from the reaction of $[Mn_3O(O_2CMe)_6(py)_3]\cdot py$ with $mpdH_2$ and NaN_3 in a 1:3:1 ratio in CH_2Cl_2. When MeCN was used, a microcrystalline solid that we were unable to further characterize was isolated.

The preparations of $(\mathbf{1})_4$ and $(\mathbf{2})_4$ are summarized in eq 1

$$40[Mn_3O(O_2CMe)_6(py)_3] + 72LH_2 + 12NaX + 4O_2 \rightarrow 3[Mn_{10}NaO_2(O_2CMe)_{13}L_6(py)_2]_4 + 84MeCO_2H + 12X^- + 96py + 24H_2O + 12H^+ \quad (1)$$

where $LH_2 = pdH_2$, $X^- = N_3^-$, OCN^-, SCN^-,$[N(CN)_2]^-$, CN^-, $(\mathbf{1})_4$; $LH_2 = mpdH_2$, $X^- = N_3^-$, $(\mathbf{2})_4$. We also investigated the use of other triangular $[Mn_3O(O_2CR)_6L_3]^{0/+}$ species, such as $[Mn_3O(O_2CEt)_6(py)_3]ClO_4$, $[Mn_3O(O_2CC(CH_3)_3)_6(py)_3]$, $[Mn_3O(O_2CPh)_6(py)_2(H_2O)]\cdot 0.5CH_3CN$, etc., as starting materials, but they only gave insoluble, amorphous precipitates that we were unable to further characterize.

Once the heterometallic nature of $(\mathbf{1})_4$ and $(\mathbf{2})_4$ and its influence on the magnetic properties had been identified (vide infra), we targeted the isolation of the homometallic Mn_{44} analogue. After preliminary variation of several reaction parameters, the desired Mn_{44} cluster with a loop-of-loops structure was successfully obtained from the reaction that gives $(\mathbf{1}\cdot 2.5CH_2Cl_2)_4$ but with $Mn(ClO_4)_2\cdot 6H_2O$ instead of a Na^+ salt. Thus, the reaction of $[Mn_3O(O_2CMe)_6(py)_3]\cdot py$ with pdH_2 and $Mn(ClO_4)_2\cdot 6H_2O$ in a 1:5:1 ratio in CH_2Cl_2 resulted in the isolation of red-brown hexagonal crystals of $\mathbf{3}\cdot(6+x)H_2O$, as well as some large reddish-brown plates that we were unable to characterize further. The large hexagonal crystals were carefully separated manually from the plates under close examination with a microscope.

Description of Structures. Partially labeled plots of complexes **1**, **2**, and the Mn_{11} loop of **3** are shown in Figure 1. The complexes all crystallize in tetragonal space groups [$I4_1/a$, $(\mathbf{1}\cdot 2.4H_2O)_4$, $\mathbf{3}\cdot(6+x)H_2O$; $P\bar{4}2_1c$, $(\mathbf{1}\cdot 2.5CH_2Cl_2)_4$; and $I4_1/acd$, $(\mathbf{2}\cdot H_2mpd\cdot 2.5H_2O)_4$] and comprise a tetrameric $\{[Mn_{10}M(\mu_3\text{-}O)_2(O_2CMe)_{13}(L)_6(L')(L'')]^{n+}\}_4$ loop-of-loops aggregate (L = pd^{2-}, L′ = L″ = py, M = Na^+, $n = 0$, $(\mathbf{1})_4$; L = mpd^{2-}, L′ = py, L″ = H_2O, M = Na^+, $n = 0$, $(\mathbf{2})_4$; L = pd^{2-}, L′ = L″ = py, M = Mn^{2+}, $n = 1$, **3**). The complexes are essentially isostructural, and thus only the structure of $(\mathbf{1}\cdot 2.4H_2O)_4$ will be described in detail and then compared briefly to the others. The structure of $(\mathbf{1}\cdot 2.4H_2O)_4$ consists of a mixed-valent loop (Figure 1A) containing two Mn^{II} and eight Mn^{III} ions, as determined by bond valence sum (BVS) calculations,[34] charge considerations, and inspection of metric parameters. The Mn ions are all in distorted octahedral geometries, with the eight

(27) (a) Altomare, A.; Cascarano, G.; Giacovazzo, C.; Guagliardi, A.; Burla, M. C.; Polidori, G.; Camalli, M. *J. Appl. Crystallogr.* **1994**, *27*, 435 SIR92. (b) Sheldrick, G. M. *SHELXL97*; University of Göttingen: Göttingen, Germany, 1997.
(28) (a) Brandenburg, K. *DIAMOND*, Version 3.1d; Crystal Impact GbR: Bonn, Germany, 2006. (b) Macrae, C. F.; Edgington, P. R.; McCabe, P.; Pidcock, E.; Shields, G. P.; Taylor, R.; Towler, M.; van de Streek, J. *J. Appl. Crystallogr.* **2006**, *39*, 453.
(29) Spek, A. L. *PLATON, A multipurpose crystallographic tool*; Utrecht University: Utrecht, The Netherlands, 2003. (b) van der Sluis, P.; Spek, A. L. *Acta Crystallogr., Sect. A* **1990**, *46*, 194.
(30) Davidson, E. R. *MAGNET*; Indiana University: Bloomington, IN.
(31) Wernsdorfer, W. *Adv. Chem. Phys.* **2001**, *118*, 99.
(32) Moushi, E. E.; Stamatatos, T. C.; Nastopoulos, V.; Christou, G.; Tasiopoulos, A. J. *Polyhedron* **2009**, *28*, 3203.
(33) Moushi, E. E.; Stamatatos, T. C.; Wernsdorfer, W.; Nastopoulos, V.; Christou, G.; Tasiopoulos, A. J. *Angew. Chem., Int. Ed.* **2006**, *45*, 7722.
(34) (a) BVS calculations for the Mn ions of $(\mathbf{1}\cdot 2.4H_2O)_4$, $(\mathbf{1}\cdot 2.5CH_2Cl_2)_4$, $(\mathbf{2}\cdot H_2mpd\cdot 2.5H_2O)_4$, and $\mathbf{3}\cdot(6+x)H_2O$ gave oxidation state values of 2.87−3.05 (Mn^{III}) and 1.96−2.11 (Mn^{II}) and revealed that the Mn_{10} loops of the $Mn_{40}Na_4$ complexes consist of eight Mn^{III} and two Mn^{II} ions, whereas the Mn_{11} loop of the Mn_{44} cluster consists of eight Mn^{III} and three Mn^{II} ions. (b) Liu, W.; Thorp, H. H. *Inorg. Chem.* **1993**, *32*, 4102.

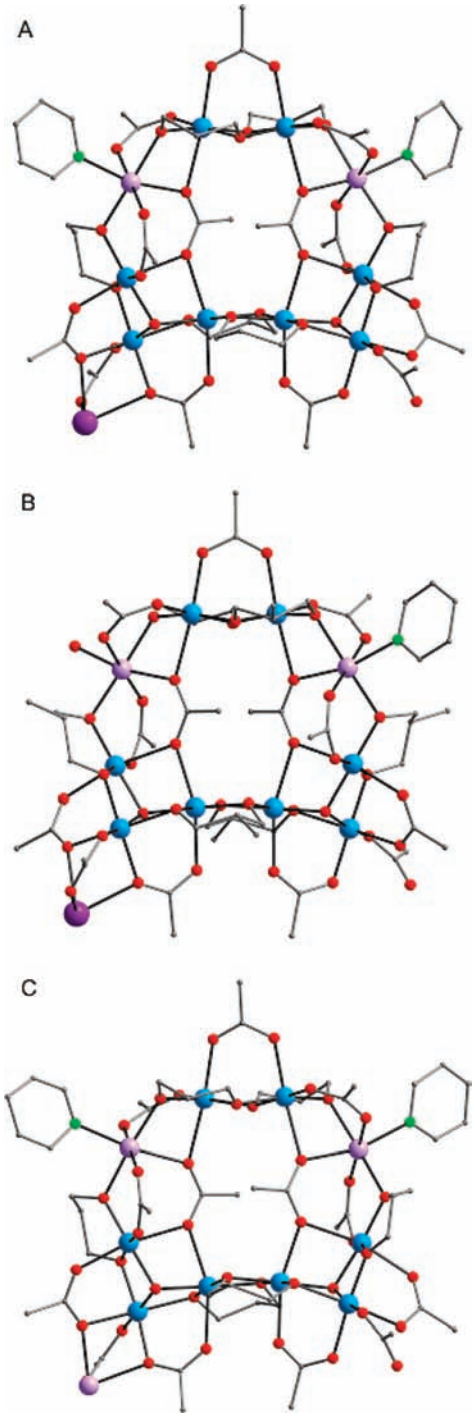

Figure 1. Molecular structures of (A) **1**, (B) **2**, and (C) the Mn_{11} loop of **3**. Color code: Mn^{III}, blue; Mn^{II}, lavender; O, red; N, green; Na, purple; C, gray. H atoms and counterions are omitted for clarity.

Mn^{3+} ions each displaying the expected Jahn−Teller axial elongation, although these are not co-parallel. The Mn_{10} loop consists of two $[Mn^{III}{}_3O]^{7+}$ triangles and two dinuclear $Mn^{II}Mn^{III}$ subunits linked by pd^{2-} μ-O atoms, and both μ-$MeCO_2^-$ and η^2:η^2:μ_4-$MeCO_2^-$ groups. The triangles are connected by two pd^{2-} μ-O atoms, whereas the $Mn^{II}Mn^{III}$ units are connected by two pd^{2-} μ-O atoms and a μ-$MeCO_2^-$ ligand. The peripheral ligation of the $Mn^{II}Mn^{III}$ subunit is completed by a μ-$MeCO_2^-$ and a pd^{2-} μ-O atom, which bridge the Mn^{II} and Mn^{III} ions, and a terminal py ligand. The Mn ions of the triangle are bridged by a μ_3-O^{2-} ion, two pd^{2-} and one acetate μ-O atoms, and two

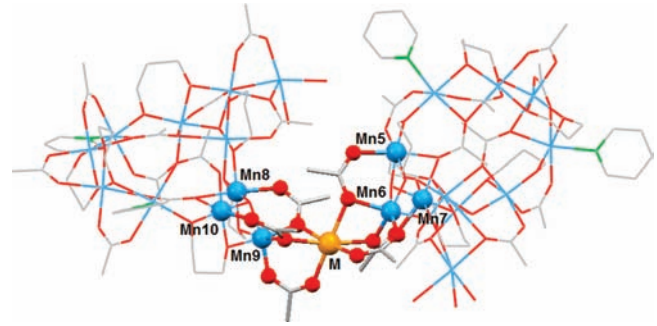

Figure 2. Part of the $Mn_{40}M_4$ ($M = Na^+$, Mn^{2+}) aggregate, emphasizing the linkage of the Mn_{10} units through the M ions to form the tetrameric cluster. Color code: Mn, blue; M, orange; O, red; N, green; C, gray. H atoms are omitted for clarity.

μ_3-$MeCO_2^-$ ligands. The latter and an additional acetate group link each triangular unit to a Na^+ ion; the two Na^+ ions attached to the Mn_{10} loop then each connect in an equivalent way to a different neighboring Mn_{10} loop (Figure 2), resulting in the formation of a large tetrameric $(\mathbf{1})_4$ loop-of-loops (Figure 3, top). This aggregate is not planar but instead folds to give a saddle-like conformation, as shown in Figure 3, bottom. All 6 propanediolate and 13 acetate ligands are fully deprotonated, as determined by BVS calculations,[35] charge considerations, and inspection of metric parameters. Four of the pd^{2-} ligands bridge two Mn^{III} and one Mn^{II} ions, and the remaining two bridge three Mn^{III} ions, all in an η^2:η^2:μ_3 fashion. In addition, all $MeCO_2^-$ ligands bridge in *syn,syn*-η^1:η^1:μ_2, η^2:η^1:μ_3, and η^2:η^2:μ_4 modes. A close examination of the crystal packing reveals that the $(\mathbf{1})_4$ aggregates pack as tail-to-tail $\{(\mathbf{1})_4\}_2$ dimers, thus giving aesthetically pleasing egg-shaped stacks (Figure 4A). The central cavity of the $\{(\mathbf{1})_4\}_2$ dimer has dimensions of approximately 8 Å × 17 Å and contains a small amount of water of crystallization. The $(\mathbf{1})_4$ units within a dimer and between different dimers are similarly spaced (the shortest Mn···Mn separation between the tails of two different $(\mathbf{1})_4$ units and between the heads of two different $(\mathbf{1})_4$ units is ∼7.68 Å).

Compound $(\mathbf{1})_4$ also crystallizes as $(\mathbf{1}\cdot 2.5CH_2Cl_2)_4$ in a different space group ($P\bar{4}2_1c$ instead of $I4_1/a$) with a different number and type of lattice solvent molecules. The molecules of $(\mathbf{1}\cdot 2.5CH_2Cl_2)_4$ pack as two layers of the type ABAB. The $Mn_{40}Na_4$ molecules of each layer have the same orientation, whereas those of different layers are not adjacent but instead are significantly shifted, resulting in the formation of a zigzag chain of $(\mathbf{1})_4$ units (Figure 4B).The crystal structure of $(\mathbf{2}\cdot H_2mpd\cdot 2.5H_2O)_4$ is very similar to that of $(\mathbf{1}\cdot 2.4\ H_2O)_4$ and differs mainly in (i) the type and number of lattice solvent molecules, (ii) the propanediolate ligand (mpd^{2-} instead of pd^{2-} in **1**), and (iii) the terminal ligation (one pyridine and one H_2O in **2** instead of two pyridines in **1**). It is interesting to note the unusually large unit cell dimensions of $(\mathbf{2}\cdot H_2mpd\cdot 2.5H_2O)_4$ (a = 34.533, b = 34.533, and c = 100.381 Å, V = 119709 Å^3), comparable to those of small proteins. The packing of $(\mathbf{2})_4$ is different than those of $(\mathbf{1}\cdot 2.4\ H_2O)_4$ and $(\mathbf{1}\cdot 2.5CH_2Cl_2)_4$. In this case, the $Mn_{40}Na_4$ units of each layer form zigzag chains which are parallel to each other in such a way that the molecules of $(\mathbf{2})_4$ are adjacent and have a tail-to-tail orientation, thus resulting in egg-shaped units along the a (Figure 4C) and b axes. The $Mn_{40}Na_4$ molecules of different layers are well separated

(35) (a) Brown, I. D.; Shannon, R. D. *Acta Crystallogr.* **1973**, *A29*, 266. (b) Donnay, G.; Allman, R. *Am. Mineral.* **1970**, *55*, 1003.

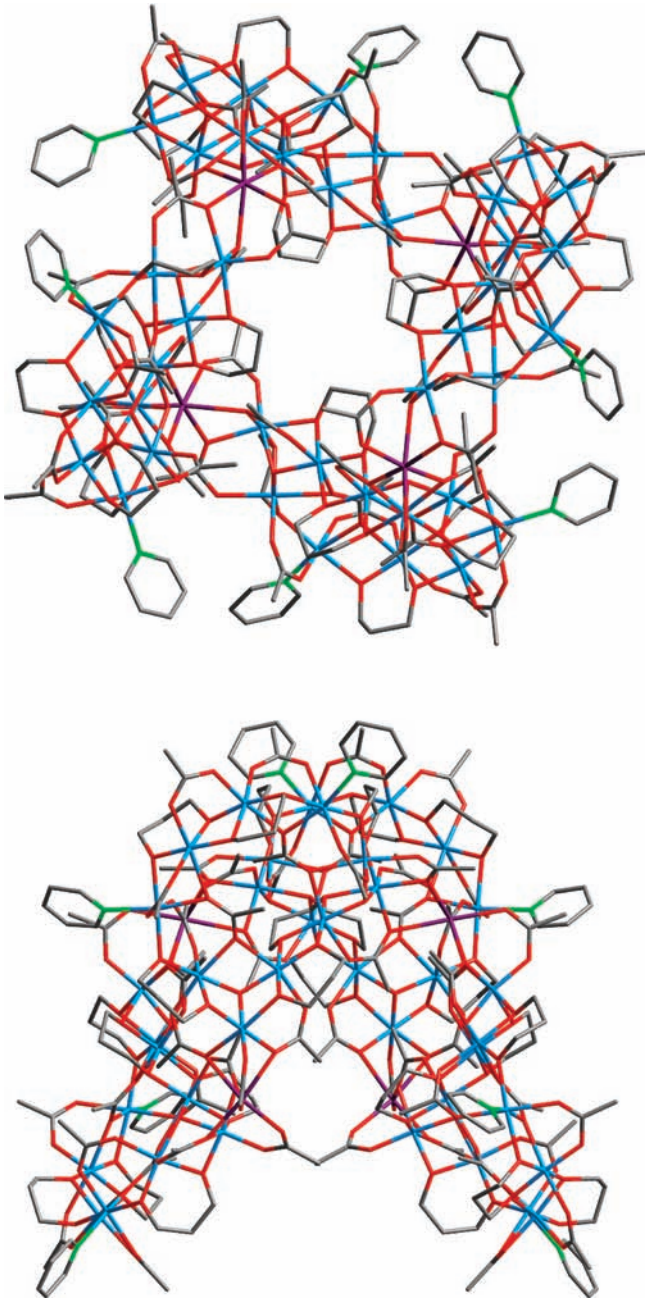

Figure 3. Wireframe representations of $(\mathbf{1})_4$ from viewpoints that emphasize (top) the tetrameric loop-of-loops structure and (bottom) the saddle-like folding. Color code: Mn, blue; O, red; N, green; Na, purple; C, gray. H atoms are omitted for clarity.

(shortest Mn···Mn separation ~9.21 Å), and thus the egg-shaped stacks do not consist of dimers of $(\mathbf{2})_4$ as was observed in $(\mathbf{1}\cdot 2.4H_2O)_4$. The neighboring units of $(\mathbf{2})_4$ within the same layer are in very close proximity (shortest Mn···Mn separation ~7.18 Å). The crystal structure of $\mathbf{3}\cdot(6+x)H_2O$ is also very similar to that of $(\mathbf{1}\cdot 2.4\ H_2O)_4$, with the main differences being that (i) the Mn_{10} loops in **3** are linked through Mn^{2+} ions, whereas those of $(\mathbf{1})_4$ are linked through Na^+ ions, and (ii) as a result, **3** is positively charged (4+), whereas $(\mathbf{1})_4$ is neutral. The packing of $\mathbf{3}\cdot(6+x)H_2O$ is very similar to that observed in $(\mathbf{1}\cdot 2.4\ H_2O)_4$, and thus supramolecular dimers of $(\mathbf{3})_2$ are also formed, with the shortest Mn···Mn separation between the neighboring units of **3** being significantly smaller (~7.10 Å) than that in $(\mathbf{1}\cdot 2.4\ H_2O)_4$ (~7.68 Å). Despite the fact that the neighboring units of **3** are in close proximity, there are no direct H-bonding interactions between them.

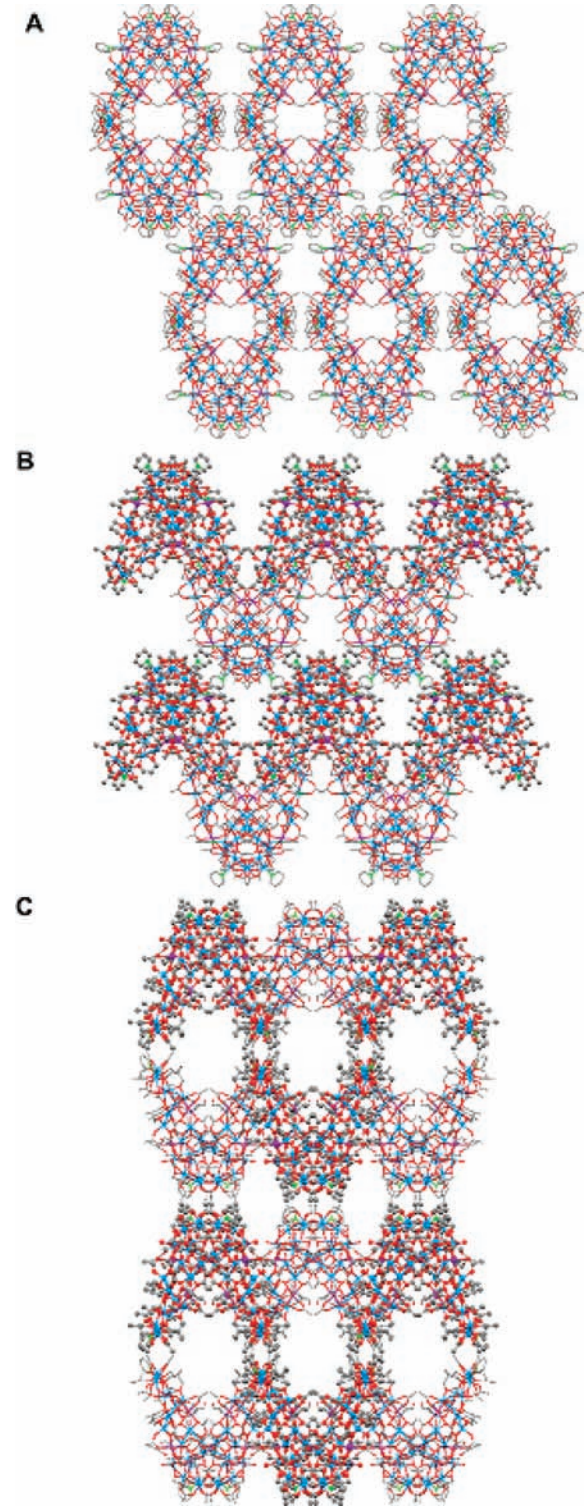

Figure 4. Representations viewed along *a* axis of the packing of (A) $(\mathbf{1}\cdot 2.4H_2O)_4$, (B) $(\mathbf{1}\cdot 2.5CH_2Cl_2)_4$, and (C) $(\mathbf{2}\cdot H_2mpd\cdot 2.5H_2O)_4$. In cases B and C, the two different types of layers are emphasized by using both wireframe and ball-and-stick representations (the same type for each layer). Color code: Mn, blue, O, red; N, green; Na, purple. H atoms and solvent molecules are omitted for clarity.

Complexes $(\mathbf{1})_4$, $(\mathbf{2})_4$, and **3** display an unprecedented structural topology, being the first examples of loops constructed from other loops. Another novel feature of the $Mn_{40}Na_4$ and

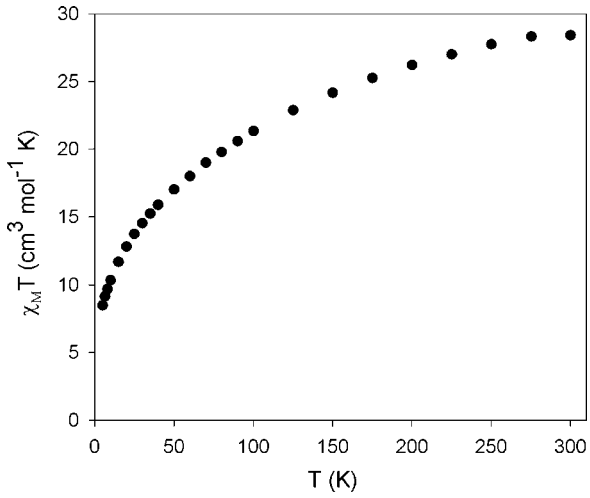

Figure 5. Plot of $\chi_M T$ vs T for $\mathbf{1}\cdot 10H_2O$.

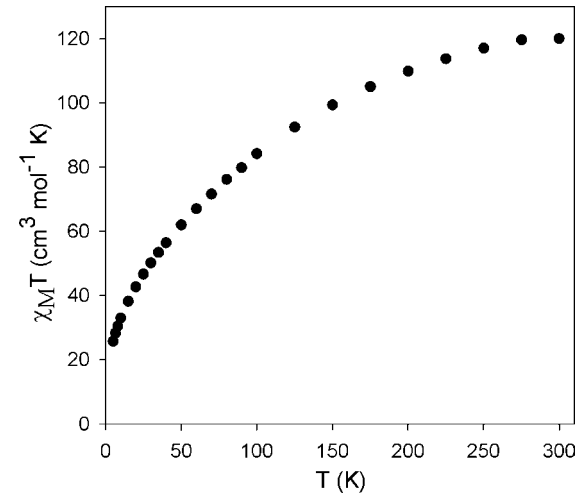

Figure 6. Plot of $\chi_M T$ vs T for $\mathbf{3}\cdot 60H_2O$.

Mn_{44} clusters is their unusually large size and nuclearity: **3** is the second largest homometallic Mn cluster, significantly larger than the Mn_{30}[9] and Mn_{32}[8] clusters and smaller only than the giant Mn_{84} torus.[7] Also, since the Na^+ ions of $(\mathbf{1})_4$ and $(\mathbf{2})_4$ are intimately associated with the Mn_{10} loops, the compounds can be considered as heterometallic $Mn_{40}M_4$ (M = any metal ion) clusters and thus possess one of the largest nuclearities observed in mixed-metal Mn_xM_y cluster chemistry.[15]

Magnetochemistry. Direct Current Magnetic Susceptibility Studies. Variable-temperature dc magnetic susceptibility (χ_M) measurements were performed on powdered polycrystalline samples of dried complexes $(\mathbf{1}\cdot 10H_2O)_4$ and $\mathbf{3}\cdot 60H_2O$, restrained in eicosane to prevent torquing, in a 1 kG (0.1 T) field and in the 5.0−300 K range. The experimental data for $\mathbf{1}\cdot 10H_2O$ and $\mathbf{3}\cdot 60H_2O$ are shown as $\chi_M T$ vs T plots in Figures 5 and 6, respectively.

$\chi_M T$ for $\mathbf{1}\cdot 10H_2O$ decreases steadily with decreasing temperature from 28.42 $cm^3\ mol^{-1}$ K at 300 K to a value of 21.34 $cm^3\ mol^{-1}$ K at 100 K, and then more rapidly to 8.48 $cm^3\ mol^{-1}$ K at 5.0 K. For complex $\mathbf{3}\cdot 60H_2O$, the $\chi_M T$ value at 300 K is 120.06 $cm^3\ mol^{-1}$ K and decreases steadily to 84.22 $cm^3\ mol^{-1}$ K at 100.00 K, and then more rapidly to 25.75 $cm^3\ mol^{-1}$ K at 5.00 K. The $\chi_M T$ values at 300 K for both complexes are significantly lower than the expected spin-only ($g = 2$) values of 32.75 and 148.5 $cm^3\ mol^{-1}$ K for $[Mn^{III}_8Mn^{II}_2]$ and $[Mn^{III}_{32}Mn^{II}_{12}]$ clusters, respectively. These data suggest the existence of strong antiferromagnetic interactions in both clusters. Furthermore, the $\chi_M T$ values at 5.0 K are in the region expected for an $S = 4$ ground state for $\mathbf{1}\cdot 10H_2O$ (spin-only value of 10 $cm^3\ mol^{-1}$ K) and an $S \approx 6-7$ ground state for $\mathbf{3}\cdot 60H_2O$ [the spin-only ($g = 2$) values for $S = 6$ and $S = 7$ are 21 and 28 $cm^3\ mol^{-1}$ K, respectively].

Given the size of the molecules, it is not possible to apply the Kambe method to determine the individual pairwise exchange interaction parameters between the Mn ions, and direct matrix diagonalization methods are also computationally unfeasible. In order to determine the ground states for both complexes, magnetization data were collected in the temperature and magnetic field ranges 1.8−10.0 K and 0.1−7.0 T (Figures S1 and S2, Supporting Information). Attempts were made to fit the resulting data using the program MAGNET,[30] which assumes that only the ground state is populated at these temperatures and includes axial zero-field splitting ($D\hat{S}_z^2$) and Zeeman interactions. However, it was not possible to obtain a good fit, and this is likely due to the existence of low-lying excited states which are populated even at the lowest temperatures employed. In fact, low-lying excited states are expected for such large molecules, in which the exchange interactions between the constituent atoms will lead to a high density of molecular spin states. In addition, as was discussed above for both complexes, there are intermolecular interactions between the neighboring units of **1** and **3** which are not incorporated in the fitting model. Such difficulty in determining the ground-state spin S from magnetization measurements has been observed in several polynuclear Mn clusters.[7,8,36−39] However, it has also been described elsewhere[8,36a,37−39] that reliable conclusions about the S value can instead be provided by ac magnetic susceptibility measurements, which also can detect the slow magnetization relaxation suggestive of SMMs. Ac susceptibility studies also preclude any complications arising from low-lying excited states in the presence of an applied dc field.

Alternating Current Magnetic Susceptibility Studies. Ac susceptibility data were collected in the 1.8−10 K range using a 3.5 G ac field oscillating at frequencies in the 5−500 Hz range. If the magnetization vector can relax fast enough to keep up with the oscillating field, then there is no imaginary (out-of-phase) susceptibility signal (χ''_M), and the real (in-phase) susceptibility (χ'_M) is equal to the dc susceptibility. However, if the barrier to magnetization relaxation is significant compared to the thermal energy (kT), then χ'_M decreases and there is a nonzero χ''_M. Such frequency-dependent χ''_M signals are a characteristic signature of the superparamagnetic-like properties of a SMM.

The in-phase and out-of-phase plots of $\mathbf{1}\cdot 10H_2O$ and $\mathbf{3}\cdot 60H_2O$ are quite similar. Thus, the $\chi'_M T$ vs T plots for both $\mathbf{1}\cdot 10H_2O$ (Figure 7) and $\mathbf{3}\cdot 60H_2O$ (Figure 8) above ~3.5 K increase steeply with increasing temperature, in agreement with

(36) (a) Murugesu, M.; Wernsdorfer, W.; Abboud, K. A.; Christou, G. *Angew. Chem., Int. Ed.* **2005**, *44*, 892. (b) Chakov, N. E.; Wernsdorfer, W.; Abboud, K. A.; Christou, G. *Inorg. Chem.* **2004**, *43*, 5919.
(37) Mishra, A.; Tasiopoulos, A. J.; Wernsdorfer, W.; Abboud, K. A.; Christou, G. *Inorg. Chem.* **2007**, *46*, 3105.
(38) Koumousi, E. S.; Manos, M. J.; Lampropoulos, C.; Tasiopoulos, A. J.; Wernsdorfer, W.; Christou, G.; Stamatatos, T. C. *Inorg. Chem.* **2010**, *49*, 3077.
(39) Stamatatos, T. C.; Nastopoulos, V.; Tasiopoulos, A. J.; Moushi, E. E.; Wernsdorfer, W.; Christou, G.; Perlepes, S. P. *Inorg. Chem.* **2008**, *47*, 10081.

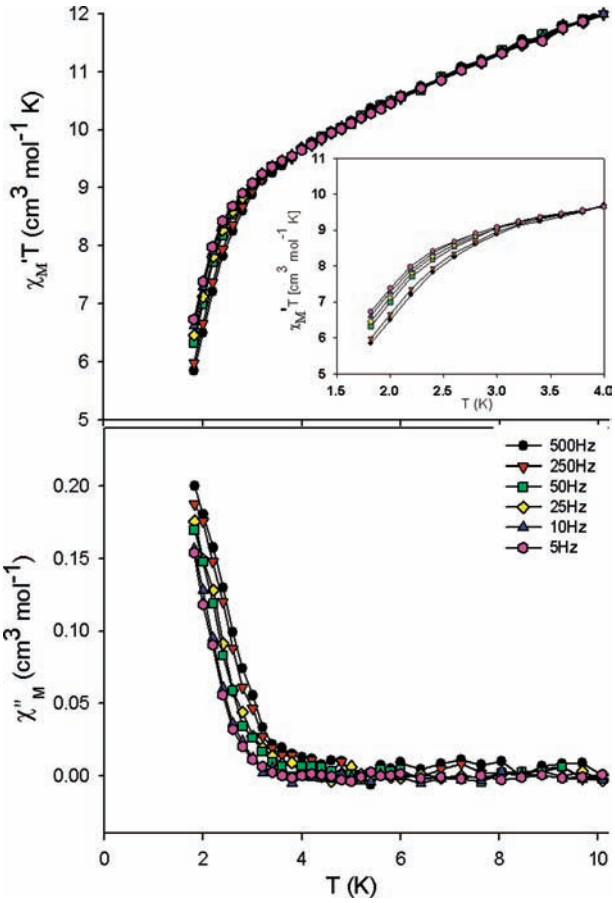

Figure 7. Plots of the in-phase (χ'_M) (as $\chi'_M T$, top) and out-of-phase (χ''_M, bottom) ac magnetic susceptibility vs T for $\mathbf{1}\cdot 10H_2O$ at the indicated frequencies. The inset in the top panel is an expansion emphasizing the frequency-dependent decrease below 4 K.

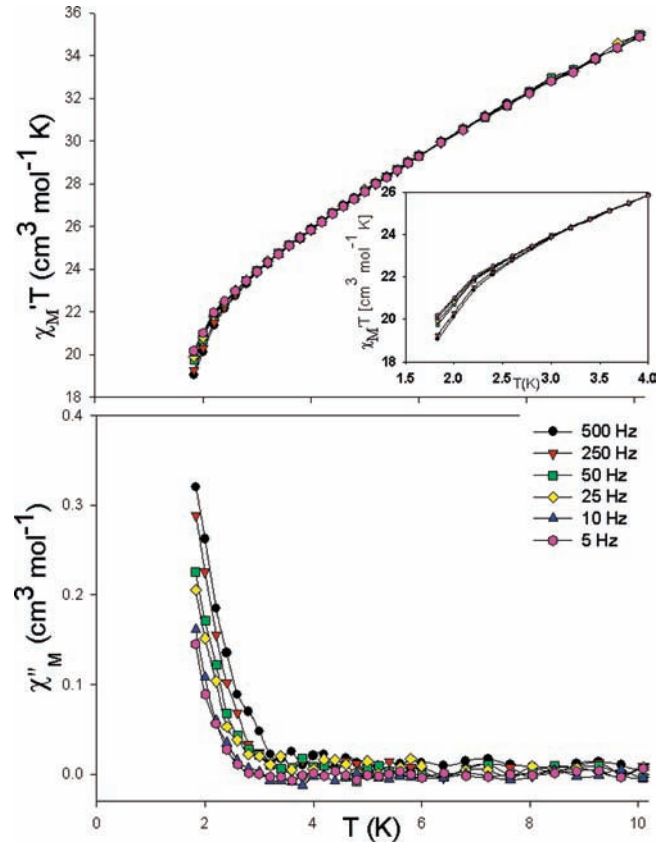

Figure 8. Plots of the in-phase (χ'_M) (as $\chi'_M T$, top) and out-of-phase (χ''_M, bottom) ac magnetic susceptibility vs T for $\mathbf{3}\cdot 60H_2O$ at the indicated frequencies. The inset in the top panel is an expansion emphasizing the frequency-dependent decrease below 4 K.

the existence of very low-lying excited states with spin greater than that of the ground state. Extrapolation of the $\chi'_M T$ versus T plots to 0 K from above ~3.5 K gives a value of ~8.5 cm^3 mol^{-1} K for $\mathbf{1}\cdot 10H_2O$ and 21 cm^3 mol^{-1} K for $\mathbf{3}\cdot 60H_2O$, indicating $S = 4$ and $S = 6$ ground states, respectively, and g values slightly less than or equal to 2.0, as expected for Mn^{III}-containing species. Below ~3.5 K, there is a frequency-dependent decrease in $\chi'_M T$ for both compounds and a corresponding appearance of frequency-dependent χ''_M signals for $\mathbf{1}\cdot 10H_2O$ and $\mathbf{3}\cdot 60H_2O$, as shown in Figures 7 and 8 (bottom), respectively; only the beginnings of peaks appear above 1.8 K, the peak maxima clearly lying at lower temperatures. The observation of out-of-phase ac signals suggested that **1** and **3** might be new SMMs, although such signals by themselves are not proof of a SMM.[37,38]

Magnetization vs Applied dc Field Hysteresis Loops. To confirm whether $(\mathbf{1}\cdot 2.4H_2O)_4$ and $\mathbf{3}\cdot(6+x)H_2O$ are indeed SMMs, magnetization vs dc field scans were carried out on single crystals using a micro-SQUID apparatus.[31] For $(\mathbf{1}\cdot 2.4H_2O)_4$, the obtained magnetization responses at different temperatures and a fixed field sweep rate of 0.070 T/s are shown in Figure 9. Hysteresis loops become evident at 4 K, but they only have a small coercivity. The latter increases, but only slightly, with decreasing temperature down to 0.04 K. This is not typical SMM behavior, for which one would expect a greater dependence of the coercivity on the temperature. We propose that this behavior is due to a combination of an intrinsic barrier to magnetization relaxation for each Mn_{10} unit and weak

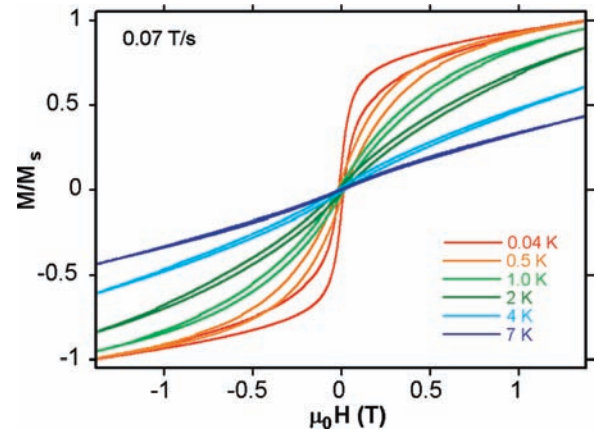

Figure 9. Magnetization (M) vs applied magnetic field ($\mu_0 H$) hysteresis loops for a single crystal of $(\mathbf{1}\cdot 2.4\ H_2O)_4$ at the indicated temperatures and a fixed field sweep rate of 0.07 T/s. The magnetization is normalized to its saturation value (M_S).

exchange interactions between the neighboring Mn_{10} units. For $\mathbf{3}\cdot(6+x)H_2O$, the obtained magnetization vs applied dc field responses are plotted in Figure 10, showing both the temperature dependence at 0.002 T/s and the scan rate dependence at 0.04 K. Hysteresis loops were now observed whose coercivities increase with decreasing temperature and with increasing field sweep rate, as expected for the superparamagnetic-like properties of a SMM. The data thus confirm complex $\mathbf{3}\cdot(6+x)H_2O$ to be a new SMM, with a blocking temperature (T_B) of ~0.7 K, above which there is no hysteresis. The hysteresis loops do not contain

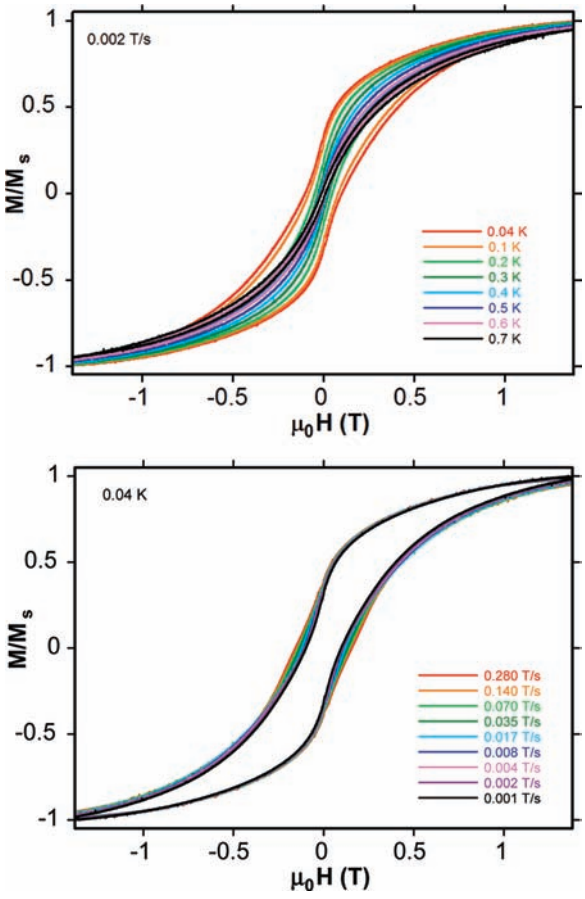

Figure 10. Magnetization (M) vs applied magnetic field ($\mu_0 H$) hysteresis loops for a single crystal of $\mathbf{3}\cdot(6+x)H_2O$ at the indicated temperatures and a fixed field sweep rate of 0.002 T/s (top) and at the indicated field sweep rates and a constant temperature of 0.04 K (bottom). The magnetization is normalized to its saturation value (M_S).

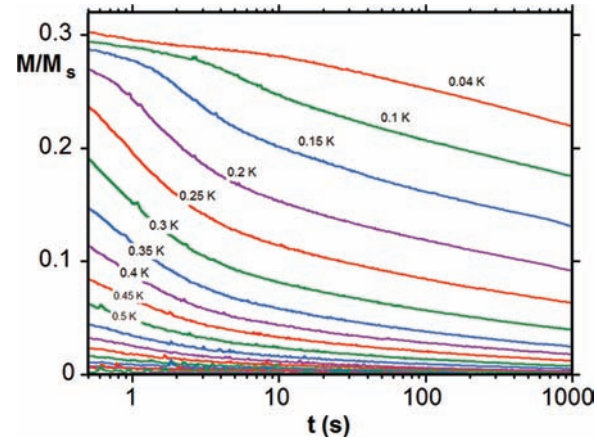

Figure 11. Magnetization (M) vs time decay plots in zero dc field for a single crystal of $\mathbf{3}\cdot(6+x)H_2O$. The magnetization is normalized to its saturation value, M_S.

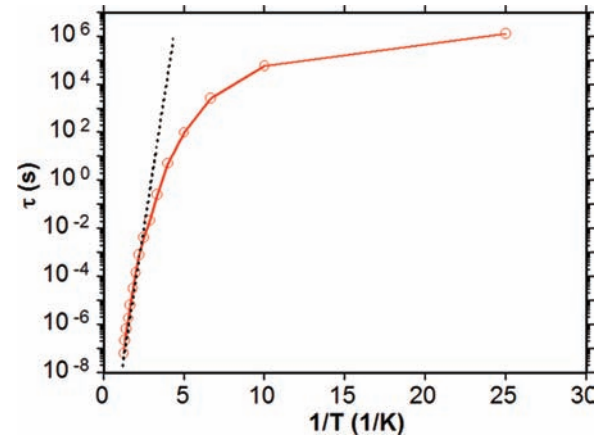

Figure 12. Arrhenius plot of the relaxation time (τ) vs $1/T$ for a single crystal of $\mathbf{3}\cdot(6+x)H_2O$ using data obtained from dc magnetization decay measurements. The dashed line is the fit of the data in the thermally activated region to the Arrhenius equation; see the text for the fit parameters.

any steps characterestic of QTM; this absence is typical for large SMMs, which are more susceptible to step-broadening effects associated with low-lying excited states, intermolecular interactions, and distributions of local environments due to ligand and solvent disorder.[7,9a,23,33,36a,39−41]

Relaxation Studies Using dc Data. Magnetization vs time decay data were collected on a single crystal of $\mathbf{3}\cdot(6+x)H_2O$ in order to obtain a more quantitative assessment of the magnetization relaxation dynamics. The sample's magnetization was first saturated in one direction at ~5 K with a large applied dc field, the temperature was decreased to a chosen value in the 0.04−0.5 K range, and then the field was removed and the magnetization decay was monitored with time. The resulting data are shown in Figure 11, from which were calculated the relaxation rates ($1/\tau$, where τ is the lifetime) at the different temperatures. These data were used to construct an Arrhenius plot, shown as τ vs $1/T$ in Figure 12, based on the Arrhenius relationship of eq 2.

$$\tau = \tau_0 \exp(U_{\text{eff}}/kT) \qquad (2)$$

The Arrhenius equation is appropriate for a thermally activated Orbach process, the characteristic behavior of an SMM, where τ_0 is the pre-exponential factor, U_{eff} is the effective relaxation barrier, and k is the Boltzmann constant. The fit to the thermally activated region above ~0.1 K gave $\tau_0 = 3.0 \times 10^{-13}$ s and $U_{\text{eff}} = 10$ K. The small value of τ_0, smaller than is typical for purely SMM behavior, is assigned to the low-lying excited states and the weak intermolecular interactions; large clusters often give smaller τ_0 values.[23a,c,39,41] Note that adjacent Mn_{44} clusters are in close proximity, but there are no direct H-bonding interactions between them, as was stated above. Thus, intermolecular exchange interactions will be rather weak, and they will represent merely perturbations of single-molecule properties. At ~0.1 K and below, the relaxation becomes temperature-independent, consistent with relaxation by ground-state QTM, i.e., via the $M_s = \pm 6$ levels of the $S = 6$ spin manifold. The above results thus establish Mn_{44} as a new giant SMM, the second largest reported to date in the literature.

Summary and Conclusions

We reported three new $Mn_{40}M_4$ (M = Na^+, $(\mathbf{1})_4$ and $(\mathbf{2})_4$, or Mn^{2+}, $\mathbf{3}$) loops constructed from four $Mn_{10}M$ loops from the use of (m)pdH_2 in Mn carboxylate chemistry. These $Mn_{40}M_4$ loops-of-loops have a saddle-like topology and crystallize in three different, aesthetically pleasing packing fashions. Magnetic studies revealed that each Mn_{10} loop of **1** has an $S = 4$ ground-

(40) Moushi, E. E.; Massello, A.; Wernsdorfer, W.; Nastopoulos, V.; Christou, G.; Tasiopoulos, A. J. *Dalton Trans.* **2010**, *39*, 4978.
(41) Murugesu, M.; Takahashi, S.; Wilson, A.; Abboud, K. A.; Wernsdorfer, W.; Hill, S.; Christou, G. *Inorg. Chem.* **2008**, *47*, 9459.

state spin and displays hysteresis loops in magnetization vs dc scans which however are not typical of an SMM due to intermolecular interactions between the neighboring Mn_{10} units. We thus targeted and achieved the preparation of a magnetically discrete homometallic Mn_{44} analogue. Magnetism studies revealed that it has an $S = 6$ ground-state spin value and unequivocally displays SMM behavior. The $S = 6$ ground state for **3** is as expected for antiferromagnetic coupling between the four $S = 4$ Mn_{10} loops and the $S = {}^5/_2$ Mn^{2+} ions that connect them, giving an overall $S = 16 - 10 = 6$ ground state for the complete Mn_{44} molecule. The Mn_{44} cluster is thus the second largest Mn cluster and SMM, being smaller in size and nuclearity only from the giant Mn_{84} torus reported recently.[7]

Further studies in progress aimed at the enhancement of the SMM behavior of **3** include synthesis of analogues with bulky carboxylate ligands to better separate the Mn_{44} units and preparation of a series of heterometallic $Mn_{40}M_4$ clusters with other paramagnetic 3d or 4f metal ions. In addition, the tetrameric $(Mn_{10}M)_4$ loop-of-loops suggests that other related aggregates of metal-linked loops or even discrete supramolecular assemblies of loops might also be possible as this work, and the chemistry of loop/wheel complexes[42] in general, is extended in the future. Finally, we recognize that the variety of supramolecular architectures of the $Mn_{40}M_4$ aggregates offers a number of possibilities for accessing interesting new compounds. Such metal−organic materials could be isolated, for example, from the covalent connection of the two units of the tail-to-tail dimers $\{(\mathbf{1})_4\}_2$ and $(\mathbf{3})_2$ that would result in a giant $Mn_{80}M_8$ aggregate, or from the insertion of guest molecules in the cavities of the loops or of the supramolecular dimers.

Acknowledgment. This work was supported by the Cyprus Research Promotion Foundation (Grant ANAVATHMISI/PAGIO/0308/12) and the U.S. National Science Foundation (CHE-0910472).

Supporting Information Available: Plots of reduced magnetization vs H/T for $\mathbf{1}\cdot 10H_2O$and $\mathbf{3}\cdot 60H_2O$ at 0.1−7.0 T and 1.8−10 K; X-ray crystallographic data in CIF format. This material is available free of charge via the Internet at http://pubs.acs.org.

JA106666H

(42) (a) King, P.; Stamatatos, T. C.; Abboud, K. A.; Christou, G. *Angew. Chem., Int. Ed.* **2006**, *45*, 7379. (b) Saalfrank, R. W.; Prakash, R.; Maid, H.; Hampel, F.; Heinemann, F. W.; Trautwein, A. X.; Böttger, L. H. *Chem.—Eur. J.* **2006**, *12*, 2428. (c) Affronte, M.; Carretta, S.; Timco, G. A.; Winpenny, R. E. P. *Chem. Commun.* **2007**, 1789.